9th Asia-Pacific Conference on Wind Engineering
Auckland, New Zealand
3-7 December 2017

Study on the Effects of Aerodynamic Interference on VIV Performance

HU Chuanxin, ZHOU Zhiyong, Zhao Lin

State Key Laboratory for Disaster Reduction in Civil Engineering

Tongji University, No.1239 Siping Road, Shanghai, China

VIV vortex-induced vibration

VEF vortex-excited force

TARS tandem arranged rectangular sections

TLR torsional lock-in region

FTLR first torsional lock-in region

STLR second torsional lock-in region

POD proper orthogonal decomposition

SSSM spring-suspended sectional model

Abstract

Based on the combination of pressure measurements and displacement measurements, mechanism of double lock-in regions of torsional vortex-induced vibration (VIV) were analysed comprehensively from the aspects of VIV responses and intrinsic mode characteristics using the proper orthogonal decomposition (POD) method. It was concluded that the interference effects on the tandem arranged rectangular sections (TARS) led to the generation of double torsional lock-in regions (TLRs). Results showed that vortex-excited force (VEF) in the downstream of upper surface and lower surface contributed mostly to total VEF of the upstream section, and VEF in the upstream of upper surface and lower surface contributed mostly to total VEFs of the downstream section, although in different TLRs. It was also found that the 1st-order and 2rd-order modes represented the VIV patterns and interference effects on TARS. The correlation regions were defined to describe interference effects on the TARS. The correlation regions of the downstream section were obviously different from those of the upstream section in different TLRs. Besides, the interference effects had a greater influence on VIV of the downstream section then that of the upstream section.

Introduction

VIV is just a typical phenomenon of wind-induced vibration, especially for the long-span bridges. The aerodynamic interference effects among multiple girder sections are one of the important factors affecting VIV performance of bridges [1-4]. Present research methods of VIV are listed as follows: theoretical analysis, field measurement, numerical simulation and wind tunnel tests. More attention has been paid to VIV responses and overall aerodynamic load effects in previous research, while ignoring distribution characteristics of VEF on the surface of models. The most obvious advantage of POD is that it can rebuild a process with a few modes which are usually related to the mechanism. The investigations of mechanisms of flutter and VIV have been comprehensively conducted by means of POD method [5-6].

Tandem arranged rectangular sections (TARS) with aspect ratio of 1: 5 were taken as the objects of this study. By means of pressure measurements and displacement measurements, with the dominant modes representing VEF based on the POD, investigation of VIV responses and dominant modes were conducted in order to get the mechanism of aerodynamic interference effects on VIV.

Experimental setup

Double rectangular sectional models with a width-depth aspect ratio of 5:1 were employed to investigate aerodynamic interference effects of tandem arranged rectangular sections on VIV performance. The approach of free vibration test of spring-suspended sectional model (SSSM) was used in this study to measure VIV responses of a single section and TARS, as shown in Figure 1. The length of the sectional models (L) was 1.74 m while the width (B) and depth (D) of the cross section was 0.30 m and 0.06 m, respectively. The horizontal net spacing between the tandem arranged sections was 360mm, vertical net spacing 0 mm, as shown in Figure 2. Besides, each section was arranged 54 pressure taps, as shown in Figure 3. The SSSM tests were carried out in a nominal smooth flow field with turbulence intensity less than 0.5%. The tested velocities ranged from 1.0 to 7.0 m/s, and the corresponding Reynolds number (Re) was between 2.03×10^4 and 4.42×10^5. All experiments were conducted in TJ-2 wind tunnel, which was a low-speed closed-circuit wind tunnel. The test section was 3.0 m wide and 2.5 m high and the wind speed could be adjusted continuously from 0.5 m/s up to 68.0 m/s.

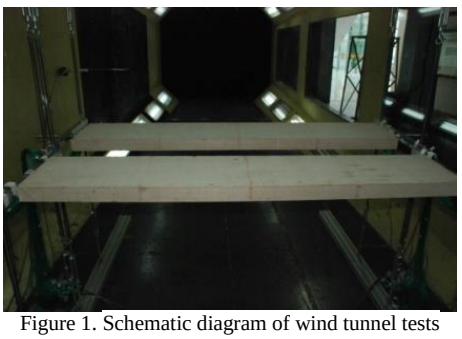

Figure 1. Schematic diagram of wind tunnel tests

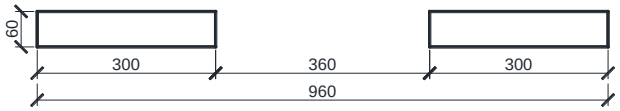

Figure 2. Geometrical sizes of tandem arranged rectangular sections (Unit: mm)

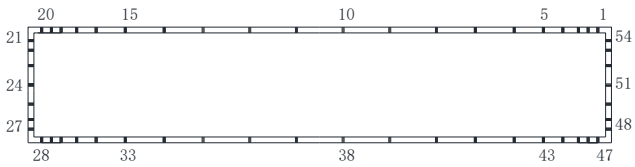

Figure 3. Layout and IDs of pressure taps

The pressure tests were carried out using the DSM3000 electronic pressure sweep valve system, PC and self-made signal acquisition software with ± 254 and ± 508mm water column produced by SCANIVALVE in the USA. The surface pressure sampling frequency was 300Hz, sampling time 40s. Each pressure tap was connected to the scanning valve by a 120cm long tube. The uniform tube length may provoke a constant phase lag of the dynamic pressure measurements for all taps. The pressure measurement signals were corrected by the frequency response function of the tubes to avoid reducing or amplifying the pressure signals. The MLS LM10-130 ANR1215 type laser displacement transducers were used to displacement measurements, it mounted 130 mm away from the target, with measuring range of 130 ± 50 mm, a resolution of 20 μm, and a linearity error of less than ± 0.2% F.S. (full scale). The main parameters of SSSM were shown in Table 1.

Total mass/(kg)		7.02
Total mass moment of inertia /(kg·m^2)		0.0958
Frequency/(Hz)	1st vertical bending	3.997
	1st torsional	8.033
Damping ratio/(%)	1st vertical bending	0.39
	1st torsional	0.41

Table 1. Main parameters of SSSM

Characteristics of VIV Responses

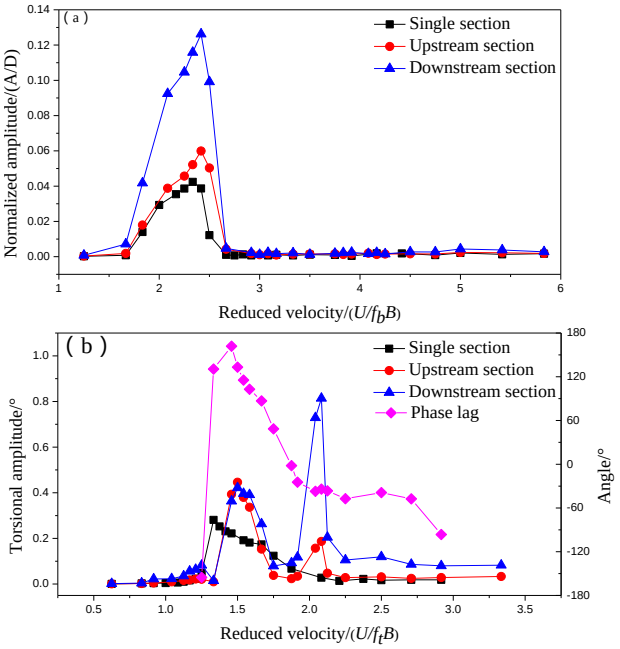

Figure 4. VIV responses of different sections. (a) vertical normalized amplitude;(b) torsional amplitude as well as phase lags between upstream and downstream sections.

The vertical and torsional VIV responses of a single section and TARS at 0° angle of attack were illustrated in Figure 4 (a) and Figure 4(b), respectively. The phase lags of displacement between upstream and downstream sections in TLRs were shown as well. It was found that there were obviously vertical VIV for each section, with the same range of reduced velocity. However, the amplitudes of responses were dramatically different, with the downstream section largest, the upstream section second, the single section smallest. The single section just had one TLR, while TARS had two. VIV responses in the first torsional lock-in region (FTLR) were nearly identical, and larger than the single section. However, VIV responses of the downstream section were much larger than that of the upstream section in the second torsional lock-in region (STLR). Additionally, it was also found that the torsional VIVs were significantly correlated with the phase lags between upstream and downstream sections, and the amplitudes of the VIV responses in FTLR and TTLR reached the maximum at the maximum value of the phase lag.

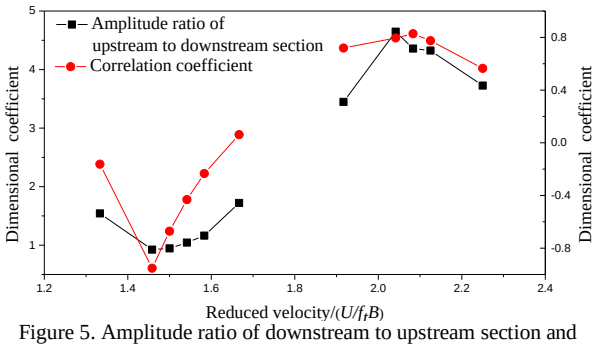

Figure 5. Amplitude ratio of downstream to upstream section and correlation coefficients versus reduced velocity

Figure 5 further showed the amplitude ratio of the downstream to upstream section and correlation coefficients between upstream and downstream sections. It indicated that VIV performances of the TARS were significantly correlated with the interference effects between them.

In general, the effects of interference on TARS could not be neglected, which directly led to the generation of double TLRs, and amplified VIV responses.

Characteristics of Intrinsic Modals

POD is a powerful tool to analyse the surface pressure of an elastic bluff body and understand the interaction mechanism between flow and bluff body [7-10]. The fluctuant pressure field can be expressed as:

$$\mathbf{C}_p(t) = \sum_{i=1}^{n} F_i(t) \tag{1}$$

$$\mathbf{F}_i(t) = \mu_i(t)\phi(i) \tag{2}$$

Where, n denotes the total number of measured pressure points; $\mathbf{F}_i(t)$ is a vector, and denotes the *i*th order mode aerodynamic force; $\mu_i(t)$ is the *i*th order principal component; $\phi(i)$ is the *i*th order mode; $\mathbf{C}_p(t)$ is a vector, and denotes the time history of fluctuant pressure, by subtraction of time-averaged pressure from measured time-varying pressure.

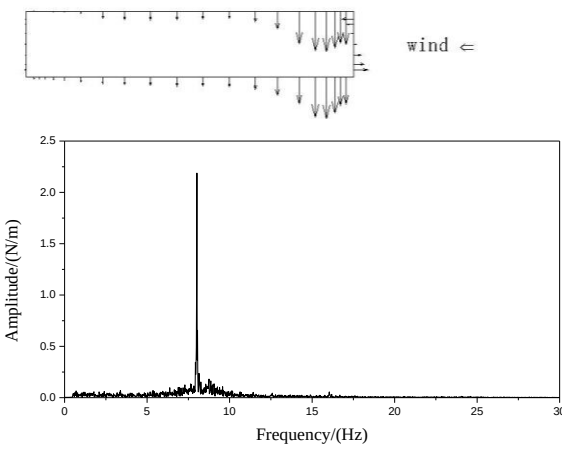

(a) The 1st-order mode

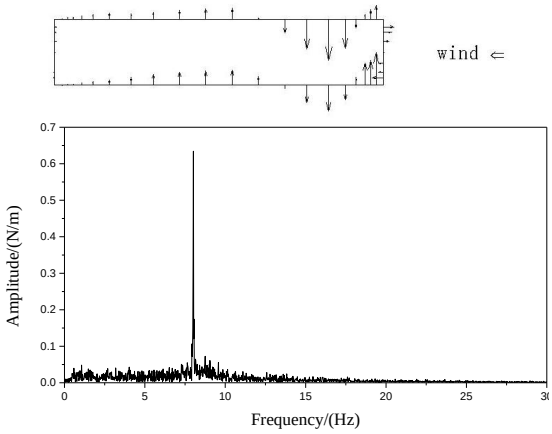

(b) The 2nd-order mode

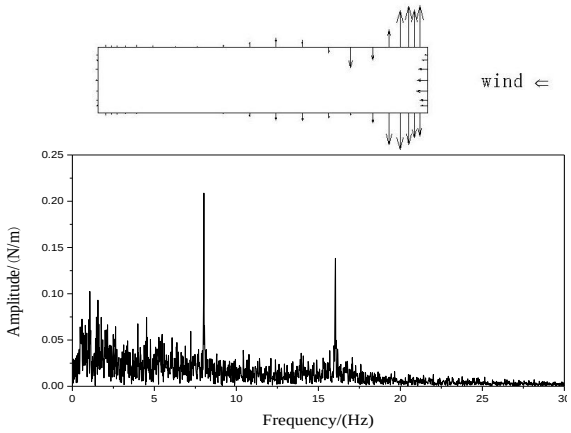

(c) The 3rd-order mode

Figure 6.The intrinsic mode and amplitude spectrum at V*=2.08

The analysed pressures were obtained at the reduced velocity of 1.50 and 2.08, representing FTLR and STLR respectively. Each section in FTLR and STLR was analysed separately by POD method.

The 1st, 2nd and 3rd mode diagram and corresponding amplitude spectrum of principal components of downstream section in STLI were shown in Figure 6. The length of lines capped with arrows in mode diagram represented the size of vector. It was observed that the dominant frequencies of all the principal components above were consistent with those of the motion of the section. Besides, the 2nd-order harmonic component was found in the amplitude spectrum of the 3rd mode, corresponding to the nonlinear characteristics of aerodynamic forces.

Case	Phase lag(°)	Error(%)	Correlation coefficient
Upstream section (V^*=1.50)	-3.4	4.1	0.98
Downstream section(V^*=1.5)	-4.6	3.7	0.99
Upstream section (V^*=2.08)	5.3	-1.8	0.99
Downstream section (V^*=2.08)	-9.7	3.4	0.98

Table 2. Relationships between the 1st order mode aerodynamic force and VEFs

Table 2 showed the relationships between the 1st order mode aerodynamic force and VEF, including phase lags, amplitude errors, and correlation coefficients. It was obvious that the phase lags were less than 10 °, amplitude errors less than 4.1 °, and correlation coefficient more than 0.98 in all cases listed. Therefore, the 1st order modes were the dominant modes, which could rebuild VEFs. However, non-linear components of VEFs were ignored. Thus, the active region of VEF, which contributed mostly to total VEFs, could be obtained in the light of the 1st order mode diagrams.

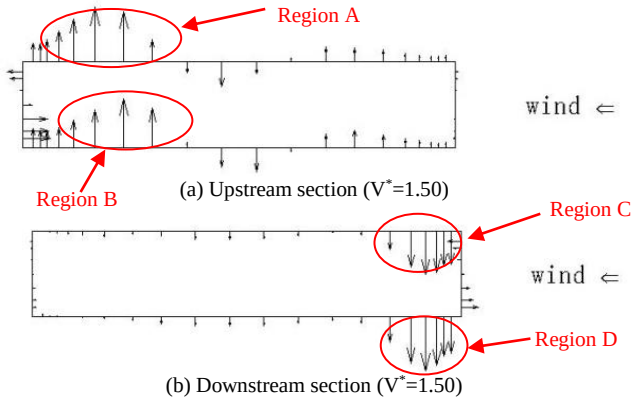

Figure 7. The 1st-order modes in different cases

As shown in Figure 7, it could be deduced that VEF in the downstream of upper surface and lower surface (Defined as A region and B region respectively) contributed mostly to total VEFs, which were the main cause of VIV of the upstream section. While the VEF in the upstream of upper surface and lower surface (Defined as C region and D region respectively) contributed mostly to total VEFs, which predominantly led to VIV performance of the downstream section.

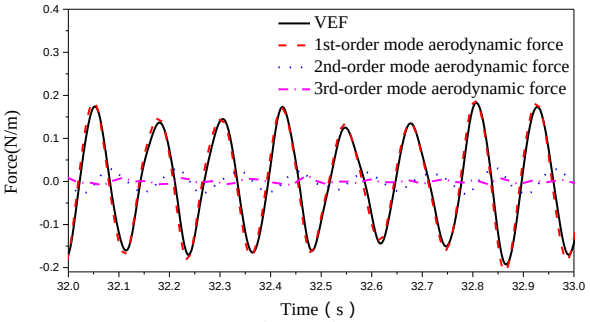

Figure 8.Time history of VEF of downstream section in STLI

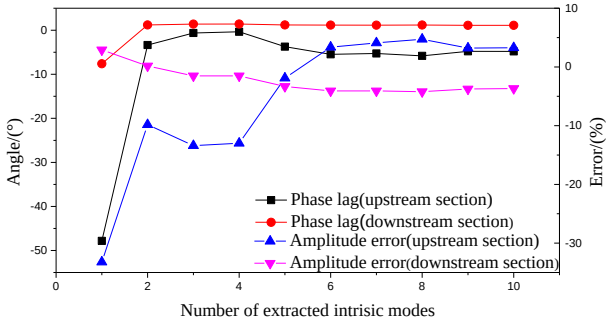

Figure 9.Phase lags and correlation coefficients between VEF and number of extracted intrinsic modal aerodynamic

In order to investigate the interference effects on TARS, TARS as a whole in FTLR and STLR were analysed by POD method. The time history of VEF, 1st-order, 2nd-order and 3rd-order mode aerodynamic forces of the downstream section in STLI were shown in Figure 8. Figure 9 showed the phase lags between mode aerodynamic forces and VEF, as well as errors between amplitude of mode aerodynamic forces and VEF in STLI. It was obvious that the phase lags were less than 4 ° and the errors of the VEF were less than 10% for the summation of the 1st-order

and 2nd-order mode aerodynamic forces. Similar conclusions were obtained in the analysis of TARS in FTLR. Therefore, the summation of 1st-order and 2nd-order mode corresponded to VIVs, which could rebuild VEFs and referred to as dominant modes. However, non-linear components of VEFs were ignored as well. Thus, the active regions of VEF could be obtained in light of the 1st and 2nd order modes.

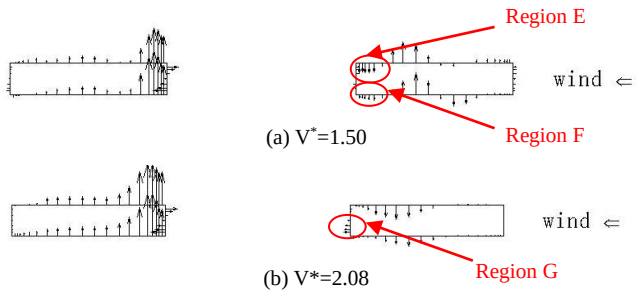

(a) V*=1.50

(b) V*=2.08

Figure 10.The 1st-order modes

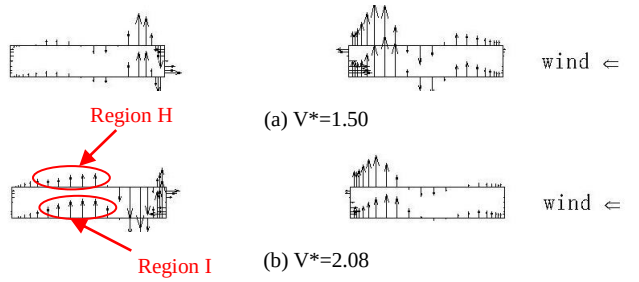

(a) V*=1.50

(b) V*=2.08

Figure 11.The 2nd-order modes

Furthermore, in accordance to the physical meaning of the intrinsic mode, VEF of each section in the same order mode was completely correlated. Thus, It was indicated that the 1st order mode characterized the interference effects of the upstream section on VEF of the downstream section, while the 2nd-order mode characterized the interference effects of the downstream section on VEF of the upstream section. So correlation regions were defined here to describe interference effects on the TARS.

As shown in Figure 10, besides middle-lower part of the lower surface and upper surface, correlation regions of the upstream section lay in the downstream of the lower surface and upper surface (Defined as region E and region F, respectively) in FTLR, while the lower part of leeward side region(Defined as region G) in STLR. Correlation regions of the downstream section were different from those of the upstream section. As shown in Figure 11, there were obviously different correlation regions in the upstream section between FTLR and STLR, especially in the middle and lower part of the upper surface and the lower surface (Defined as region H and region I, respectively).

Since the 1st-order mode contributed much more to the VEF than the 2nd order mode, it was concluded that the interference effects had a greater influence on VIV of the downstream section than that of the upstream section.

Conclusions

In this paper, the mechanism of double TLRs was analysed comprehensively from the aspects of VIV responses and intrinsic mode characteristics by means of pressure measurements and displacement measurements. It was concluded that the interference effects between the upstream and downstream sections led to the generation of double TLRs. Results showed that VEF in the downstream of upper surface and lower surface contributed mostly to total VEF of the upstream section, while VEF in the upstream of upper surface and lower surface contributed mostly to total VEFs of the downstream section, although in different TLRs. It was also found that the 1st-order and 2nd-order modes represented the VIV patterns and interference effects between the downstream and upstream section. Correlation regions were defined here to describe interference effects on the TARS. Correlation regions of the downstream section were obviously different from those of the upstream section in different TLRs. The interference effects had a greater influence on VIV of the downstream section than that of the upstream section.

Acknowledgments

References

[1] Honda A, Shiraishi N, Matsumoto M, et al. Aerodynamic stability of Kansai International Airport access bridge [J]. Journal of Wind Engineering & Industrial Aerodynamics, 1993, 33(1-2):369-376.

[2] Kim S J, Kim H K, Calmer R, et al. Operational field monitoring of interactive vortex-induced vibrations between two parallel cable-stayed bridges [J]. Journal of Wind Engineering & Industrial Aerodynamics, 2013, 123(4):143-154.

[3] Seo J W, Kim H K, Jin P, et al. Interference effect on vortex-induced vibration in a parallel twin cable-stayed bridge [J]. Journal of Wind Engineering & Industrial Aerodynamics, 2013, 116(116):7-20.

[4] Argentini T, Rocchi D, Zasso A. Aerodynamic interference and vortex-induced vibrations on parallel bridges: The Ewijk bridge during different stages of refurbishment [J]. Journal of Wind Engineering & Industrial Aerodynamics, 2015, 147:276-282.

[5] Carassale L, Solari G, Tubino F. Proper orthogonal decomposition in wind engineering-Part 2: Theoretical aspects and some applications [J]. Wind & Structures An International Journal, 2007, 10(2):177-208.

[6] HU Chuan-xin, YANG Li-kun, ZHOU Zhi-yong. Research on Vortex Vibration of Bridge Based on POD and Dynamic Pressure Measurement [J]. Chinese Quarterly of Mechanics, 2013, 34(4):591-598.

[7] Amandolésea X, Crémona C. Analysing fluid loadings on moving bluff bodies using proper orthogonal decomposition. J Fluids Struct 2005; 52:577-87.

[8] Tamura Y, Suganuma S, Kikuchi H, Hibi K. Proper orthogonal decomposition of random wind pressure field. J Fluids Struct 1999; 13:1069-95.

[9] Ricciardelli F. On the wind loading mechanism of long-span bridge deck box sections. J Wind Eng Ind Aerodyn 2003; 91: 1411-30.

[10] Tubino F, Solari G. Gust buffeting of long span bridges: double modal transformation and effective turbulence. Eng Struct 2007; 29: 1698-707.